The International Supercritical CO_2 Energy Technologies Symposium
March 2 - 5, 2026, Pittsburgh, PA
Paper #031

Process Improvement Using CO_2 Turbine Expanders

Nick Bogan
Senior Engineer
Ebara Elliott Energy
Jeanette, PA

August Brautigam
Senior Engineer
Ebara Elliott Energy
Jeanette, PA

Enver Karakas
Fellow Engineer
Ebara Elliott Energy
Jeanette, PA

Nick Bogan is a Research and Development Engineer with Ebara Elliott Energy, where his current focus is on the design of liquid and two-phase expanders for cryogenic service. He began his career as a Project Engineer at Ebara Elliott Energy before pivoting to robotics, spending 7 years with Hamilton Company designing medical equipment for laboratory automation. He's now returned to Ebara Elliott Energy in a research and development role, where he's working to improve energy transport efficiency and develop new and improved methods of energy conservation. Nick has a Master of Science Degree in Mechanical Engineering from the University of Nevada, Reno, where his main focus was on two-phase heat transfer.

August Brautigam is a Research and Development Engineer at Ebara Elliott Energy, where he is currently focused on the design of ammonia pumps and expanders. He began his career in rotating machinery as an Organic Rankine Cycle Systems Engineer dealing with two-phase screw expanders for ElectraTherm. He then worked as a Project Engineer and later a Research and Development Engineer at Ebara Elliott Energy. He spent seven years designing medical equipment for laboratory automation at Hamilton Company and has returned to Ebara Elliott Energy to pursue his long-standing interest in turbomachinery. His primary areas of focus include thermodynamic analysis of power cycles, two-phase power recovery, and renewable energy production.

Enver Karakas is a distinguished Fellow Engineer and Senior Manager of Pump and Hydraulic Expander Development Division with over 20 years of experience in design and development of turbomachinery for oil and gas applications. Enver has been working for Ebara Elliott Energy since 2003. Enver specializes in cryogenic pump and hydraulic turbine technologies and is responsible for product development, testing and troubleshooting of cryogenic rotating equipment. Enver has Master of Science and a Doctorate Degree in Mechanical Engineering from the University of Nevada, Reno. He has been a research associate with University of Nevada, Reno and has established and led Turbomachinery Laboratory at University of Nevada, Reno where he studied and investigated cavitation performance of cryogenic centrifugal pumps and multiphase flow in cryogenic turbines.

1. ABSTRACT

As global energy demand continues to increase, the need for alternative energy sources and processes has gained attention. Whether through pre-combustion refinement, post-combustion carbon capture, utilization, and storage (CCUS), or as the working medium in large scale heat pump applications, carbon dioxide plays an important role in this evolving energy ecosystem. In each of the aforementioned processes, it is necessary for high pressure CO_2 liquid to be expanded, either for transport or energy extraction. This expansion is traditionally achieved through use of a Joule-Thomson (J-T) valve. The implementation of CO_2 liquid or two-phase expanders in place of the typical J-T valve works to improve process and plant efficiency in two ways. First, because the expander extracts work from the fluid in the form of shaft power, additional cooling by enthalpy reduction is realized, which in turn increases the amount of liquid retained during the expansion process. Second, this extracted shaft power can be used to offset power demands of other machinery in the loop or be fed back into the power grid, further increasing overall process efficiency. This paper details the current state of CO_2-driven processes in an ever-growing global energy economy and emphasizes the role that liquid and two-phase CO_2 expanders will play in improving the efficacy of these processes. Operational characteristics and overall turbomachinery design are discussed. Liquefaction and large-scale heat pump processes using the traditional Joule-Thomson expansion valve are compared to expansion via liquid and two-phase expanders. Production gains and electrical regeneration benefits are quantified.

2. INTRODUCTION

Cryogenic liquid and two-phase expanders mitigate the inefficiency of traditional throttled expansion by extracting energy from the fluid as it expands — providing additional cooling by enthalpy reduction and generating electrical energy. In LNG liquefaction, implementation of cryogenic expanders in place of traditional throttling valves can convert up to 3 MW of gas otherwise boiled off into electrical energy and appreciably increase liquid throughput. Adaptation of this technology to CO_2 liquefaction and power cycles can provide similar gains to the emerging carbon capture, utilization, and storage (CCUS) market. Many fundamental energy-driven processes emit greenhouse gases like CO_2 as a byproduct, and the increasing global energy demand has made the CO_2 market an area of focus in the energy sector. In 2022, CO_2 accounted for nearly 80% of all greenhouse gas emissions [1]. The need to efficiently capture, utilize, and/or store this excess carbon dioxide is critical to the foundation of a decarbonized economy and the use of cryogenic expanders to boost the efficiency of CO_2-driven processes will add to the long-term efficacy of this developing energy infrastructure.

3. BACKGROUND

3.1. Carbon Capture, Utilization, and Storage (CCUS) Using Liquid Expanders

Carbon capture, utilization and storage (CCUS) is a direct means of minimizing the amount of CO_2 released into earth's atmosphere and is an integral part of many industrial processes. Technologies to separate and capture CO_2 from flue gas streams are commercially available. As of May 2023, over 8 million tons of CO_2 had been captured and stored [2]. These separation and capture processes are energy intensive, however, and efforts to improve their efficiency are important to minimize the net energy demand as well as their resulting environmental impact.

In this section, post-combustion CO_2 capture processes are reviewed. The focus is on where liquid expanders can be utilized to improve process efficiency in terms of energy recovery and

more importantly, in CO_2 production. Three commonly used post-combustion processes are discussed, namely chemical absorption (amine scrubbing), membrane separation, and cryogenic separation. Each process focuses on CO_2 capture from flue gas which contains CO_2, N_2, O_2 and H_2O with various contaminants after combustion.

3.1.1. Chemical Absorption (Amine Scrubbing) Process

This is the most common post-combustion CO_2 capture process. The process is designed around two large chemical contact columns connected by heat exchangers and pumps. There are four main steps to this cycle. It operates in a continuous loop to capture CO_2 from an industrial source, such as a power plant's flue gas, and prepare it for transport and storage. A typical schematic view of this process is shown in Figure-1.

The first step is pre-treatment and cooling. Contaminants such as acid gases — namely sulfur dioxide SO_2, sulfur trioxide SO_3, and hydrogen chloride HCl — Nitrogen oxides, and oxygen are removed from the flue gas. Pre-treatment is a critical part of the process because the solvents used, particularly amine solutions, are highly sensitive to various impurities often found in the flue gas. The flue gas enters a Direct Contact Cooler (DCC), where it is cooled, typically to 40-50°C. The purpose is to match the optimal temperature of the amine solvent and prevent excessive water loss from the solvent.

The second step is absorption (capture). The pre-treated flue gas enters the bottom of the Absorber Column and flows in an upward direction. At the same time, cold, regenerated lean solvent, which is very low in CO_2 concentration, enters the top of the column and flows downward in counter-current flow, trickling over packing material or trays to maximize the contact area. The solvent chemically reacts with the CO_2 to form a stable, soluble compound, which is the carbamate for primary/secondary amines. The treated flue gas, now free of CO_2, exits the top of the column and is vented to the atmosphere. The solvent, now with a high concentration of CO_2, exits at the bottom as "rich solvent".

The third step is heat exchange and regeneration, also known as stripping. At this step, CO_2 rich solvent is pumped through the Rich/Lean Heat Exchanger, where it is preheated by the outgoing hot lean solvent, significantly reducing the external heat input needed. The hot CO_2 rich solvent is then fed into the top of the stripper (regenerator) column and flows downward. Additional heat to the CO_2 rich solvent is supplied at the bottom of the stripper by the reboiler. The reboiler is often supplied with heat from the power plant's low-pressure steam. High temperature and lower pressure in the stripper reverse the chemical reaction, breaking the chemical bond between CO_2 and the solvent.

The final step is CO_2 capture and solvent recycling back to the absorber. High-purity CO_2 and water exit the top of the stripper. The stream is cooled to condense and separate the water via a cooler and a separation vessel, leaving a concentrated stream of CO_2 ready for compression, transport, and storage or utilization. Now the solvent must be recycled back to the process. The hot regenerated lean solvent exits the bottom of the stripper, passes through the Rich/Lean Heat Exchanger, and is finally cooled down to the absorber's inlet temperature before being pumped back to the top of the absorber column to restart the cycle.

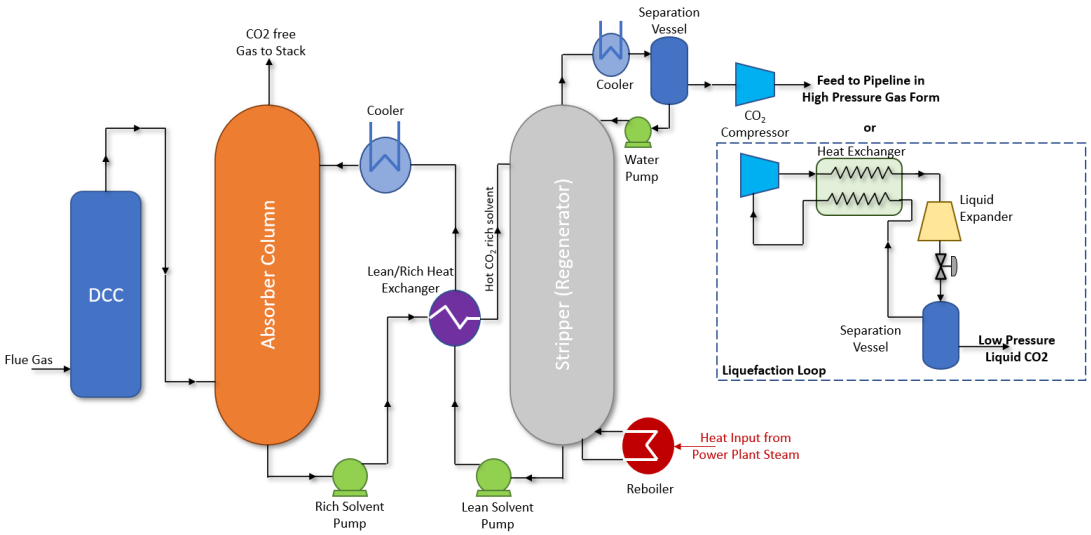

Figure-1 Chemical Absorption Process with Simple Liquefaction Loop

For transportation or storage, the CO_2 stream is fed to a compressor to increase the pressure. This pressurized stream is then suitable for either cooling and liquefaction (for storage) or for transportation in a pipeline as supercritical CO_2 (sCO_2).

CO_2 in vapor form can be fed to a simple refrigeration loop, as shown in Figure-1, for liquefaction and safe storage under low pressure. A liquid expander is utilized to reduce the CO_2 pressure to an acceptable level. While the main purpose of the expander is to reduce the pressure of CO_2, an expander can also recover the lost energy and increase the liquid production rate by providing additional cooling. This considerably improves the liquefaction process efficiency.

3.1.2. Membrane Separation Process

A membrane separation process uses a selective barrier (membrane) to physically capture CO_2 from other gases after combustion. The separation is achieved based on the principles of differential permeation. Differential permeation is fundamentally allowing one gas to pass through the membrane much faster than the others. In the case of membrane separation of CO_2, CO_2 passes through the membrane much faster than the other gases (N_2 and O_2). Figure-2 is a simple schematic view of the membrane separation for CO_2 capture.

Flue gas is fed to a pretreatment unit to remove containments. The pretreatment unit consists of particulate filters and electrostatic precipitators to remove sulfur oxides and dust or fly ash, respectively. A de-NO_x unit may be present to remove any NO_x before or after CO_2 capture depending on the plant design.

As shown in Figure-2, the pressure of the flue gas is increased via feed compressor prior to entering to the first membrane unit. This enhances the partial pressure driving CO_2 across the membrane, improving the efficiency and the amount of gas passing through. The membrane is the core of the process and it houses the actual membrane material. As the feed gas flows through the membrane unit, CO_2 permeates the membrane while N2 and other non-permeating gasses are retained. To assist in differential permeation, a vacuum pump can be used downstream of the membrane unit to further increase the differential pressure, thereby

enhancing CO_2 recovery. The gas that did not permeate the membrane is now depleted in CO_2 and mainly consists of N_2. The process can be utilized in stages and can have multiple membrane units, as shown in Figure-2. The captured CO_2 stream can be pressurized via a compressor for pipeline transportation or can be liquefied similar to the cycle described in the chemical absorption process.

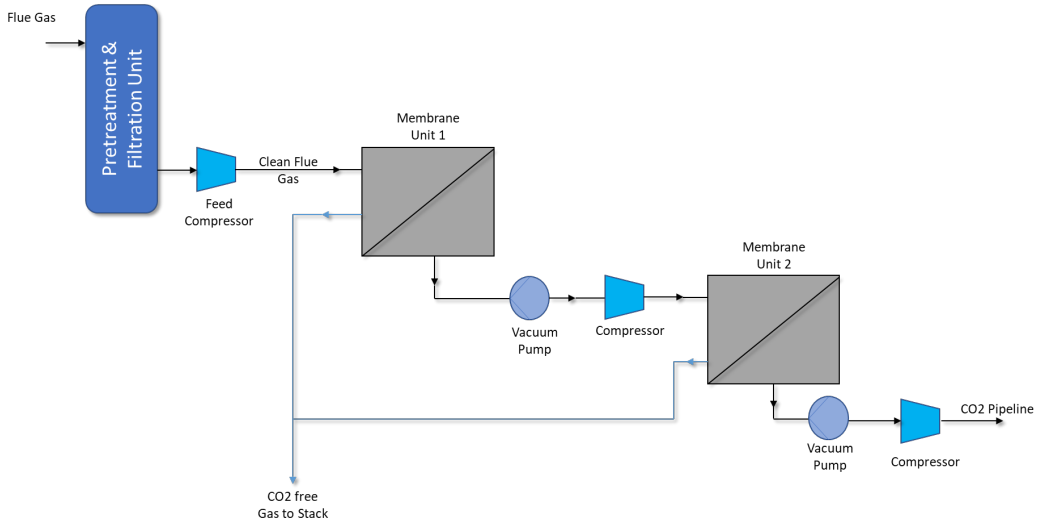

Figure-2 Typical Membrane Separation Process for CO_2 capture

3.1.3. Cryogenic Capture Process

The cryogenic capture process separates CO_2 from flue gas by cooling the gas stream to extremely low temperatures. Cooling causes the CO_2 gas to change directly to liquid or solid phase, which can then be physically separated. This method relies on the difference in freezing and condensation points of CO_2 and other gasses like N_2 and O_2. It should be noted that CO_2 desublimates around -100 to -135°C depending on its feed pressure. Therefore, cooling CO_2 to these low cryogenic temperatures is crucial for this process. A schematic view of this process is shown in Figure-3.

Initially the hot flue gas stream is cooled down to near ambient temperature. This initial cooling allows most of the water vapor to condense and to be removed from the flue gas. This step is important because water turns into ice at 0°C and would quickly clog the cold sections of the system. Besides water, many pollutants, such as sulfur dioxide and hydrogen chloride, which have higher freezing points than CO_2, are also removed from the feed gas. This is a major difference and advantage in the cryogenic process as it often eliminates the need for separate SO_x and NO_x removal. After cryogenic cooling at temperatures between -100 and -135°C, CO_2 in the gas stream bypasses the liquid phase and freezes directly intro solid CO_2 particles (dry ice).

Once the CO_2 has solidified, it is physically separated from the remaining gas, which is primarily N2. These CO_2 depleted gases are then vented back to the atmosphere. The captured solid CO_2 is then prepared for transport and storage. It is pressurized via solid handling system or a pump and then melted and warmed in heat exchangers. These pressurization, melting and warming processes transform the dry ice to a high purity, pressurized liquid CO_2 stream. It is crucial to get solid CO_2 to a pressure above its triple point

before melting since dry ice does not melt at atmospheric pressure. To increase the pressure of CO_2 solid, a small amount of CO_2 liquid is mixed with the solid to form a pumpable slurry; a screw conveyor or solids compactor may also be used. The outcome is a high-pressure CO_2 liquid stream at the end of the process. If the pressure must be reduced for transportation and storage, a liquid expander can be utilized to achieve acceptable pressure levels, while the lost energy during expansion process is recovered.

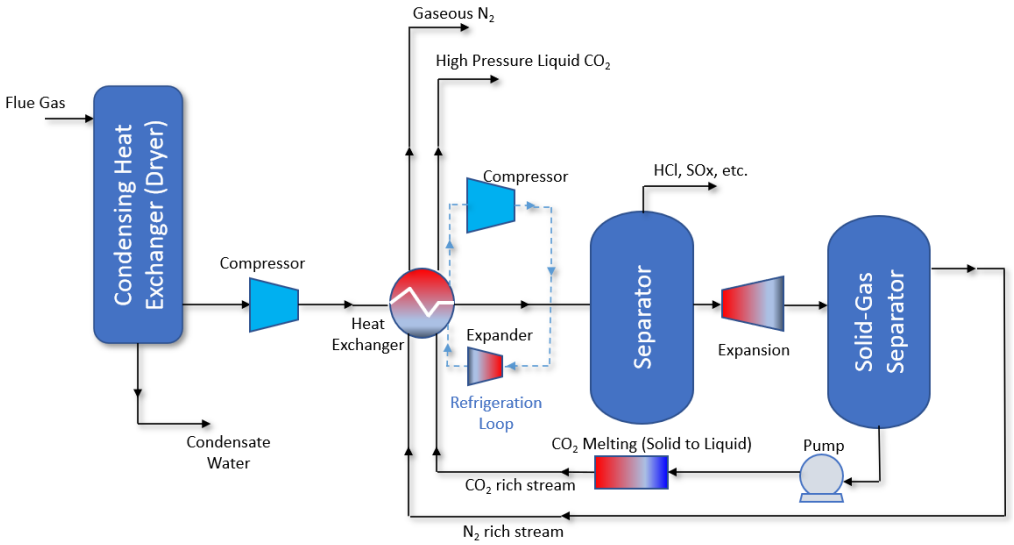

Figure-3 Typical Cryogenic Capture Process for CO_2

3.2. Large Scale Heat Pump Applications

Supercritical carbon dioxide can be used as the working fluid in large scale heat pump applications for power grid energy management [3]. Heat pump energy storage is known as Pumped Thermal Energy Storage (PTES), and it can be used as a non-geographically-limited peak shaving option. McTigue et al. compare PTES to Pumped Hydroelectric Storage (PHS), Compressed Air Energy Storage (CAES), and Li-ion battery storage. While PHS requires a ready supply of water, a mountain to pump it up, and a reservoir to store it in, PTES typically requires only compressors, pumps, turbines, and heat exchangers. Like PHS, CAES requires a large physical reservoir, in this case an airtight underground cavern. Li-ion battery storage can be readily employed and is insensitive to geography, but the capital cost is $200-$800 per kWh, considerably higher than the PTES capital cost of $25-$250 per kWh [3].

A typical sCO_2 heat pump charge cycle is shown in Figure-4. In this example, drawing approximate state definitions from [3], the high-side pressure is approximately 218 bar absolute and the low system pressure is set to 80 bar to keep the fluid in a supercritical state. The CO_2 working fluid is compressed from 80 bar and 100°C in state 1 to 218 bar and 300°C in state 2. Heat is rejected to the source at 216 bar between states 2 and 3, allowing for a 1% pressure drop in the heat exchanger. Power is then extracted through a liquid turbine during the pressure letdown process between states 3 and 4, offsetting some of the compressor power consumption. Heat is absorbed from the sink, which is described in [3] as a synthetic fluid operating at a temperature difference of 5°C between the storage fluid and the process fluid, between states 4 and 1.

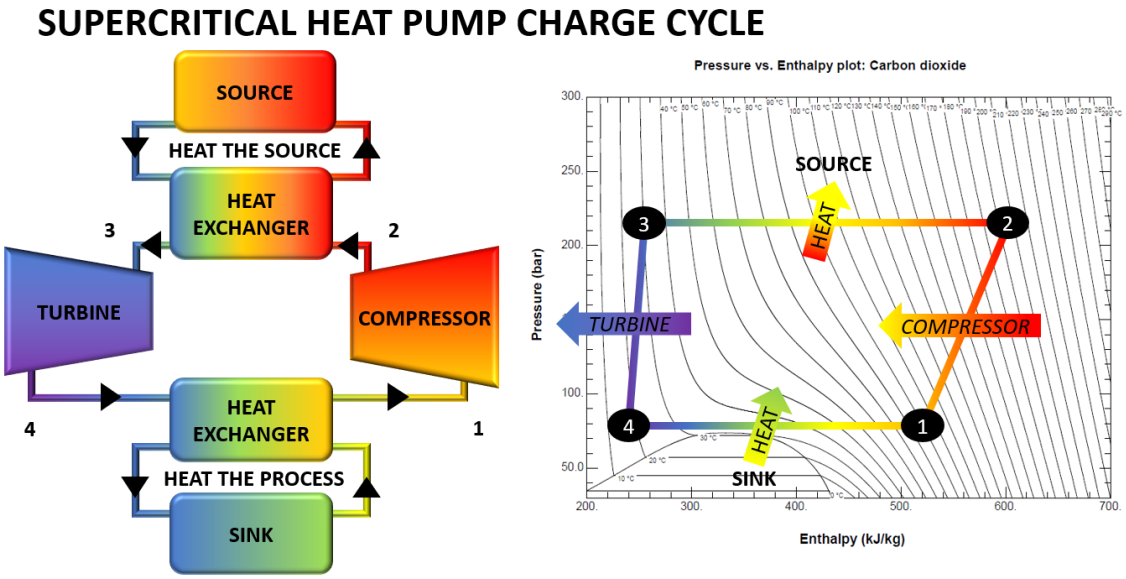

Figure-4 Supercritical heat pump charge cycle

Heat stored during the heat pump cycle in Figure-4 is recovered through the use of a Brayton cycle as shown in Figure-5. This heat recovery is performed during peak hours, when electricity is most expensive or least readily available. The discharge process is a typical supercritical Brayton cycle. CO_2 is compressed from 80 bar and 27.7°C to 195 bar and 45°C. Heat is added from the source, which is at 195°C at the outlet, allowing a maximum temperature of 190°C at state 3 on the process side. Power is extracted from the fluid via a turbine from state 3 to 4, dropping the pressure to 80.8 bar at state 4, 1% greater than the 80 bar datum at state 1. Heat is then rejected to the sink between state 4 and 1.

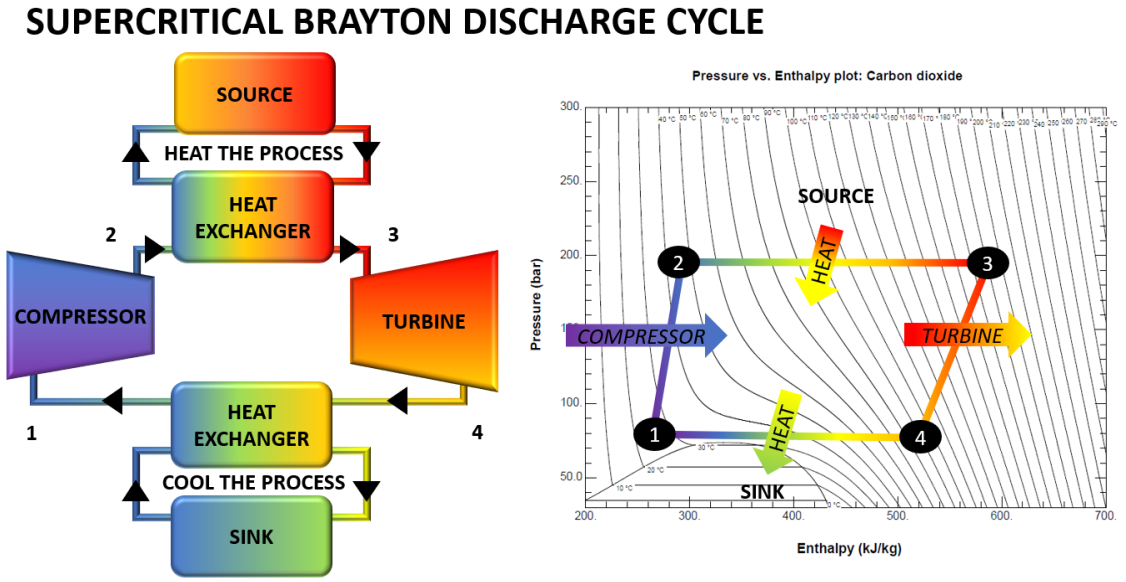

Figure-5 Supercritical Brayton Discharge Cycle

Given a constant temperature heat sink such as ocean water, a high-temperature thermal reservoir, a turbine, and a compressor, a transcritical charge cycle may be constructed as shown in Figure-6. From state 1 to 2, a compressor increases the pressure and temperature of the gas phase of CO_2. This high pressure, high temperature fluid is then used to heat the source between states 2 and 3. The low temperature, high pressure CO_2 is then expanded through a Francis (liquid) turbine between states 3 and 4, allowing for recovery of electric power. The temperature of the working fluid is now below the temperature of the sink, allowing heat to be added to the process between states 4 and 1 prior to compression.

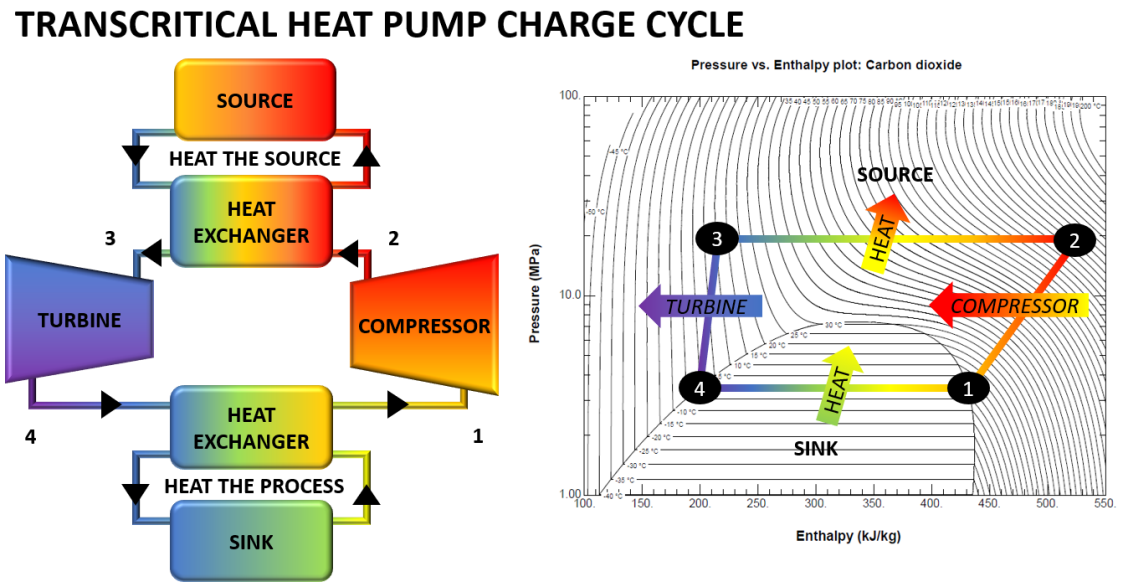

Figure-6 Transcritical Heat Pump Charge Cycle

Given the same sink and source, the transcritical heat pump cycle may be reversed and may be operated as an Organic Rankine Cycle (ORC) as shown in Figure-7. This reversal requires a pump in the place of the liquid turbine shown in Figure-6, and a gas turbine in the place of the gas compressor shown in Figure-6. From state 1 to 2, cold CO_2 is pumped to the high system pressure. From state 2 to 3, the sCO_2 is heated by the source to the high temperature in the system. The hot fluid is then expanded through a gas-phase turbine from state 3 to 4, extracting energy that was stored during the charge cycle. Heat is then rejected from the fluid between state 4 and 1. In this case, the CO_2 is above the temperature of the sink, allowing heat rejection prior to recompression.

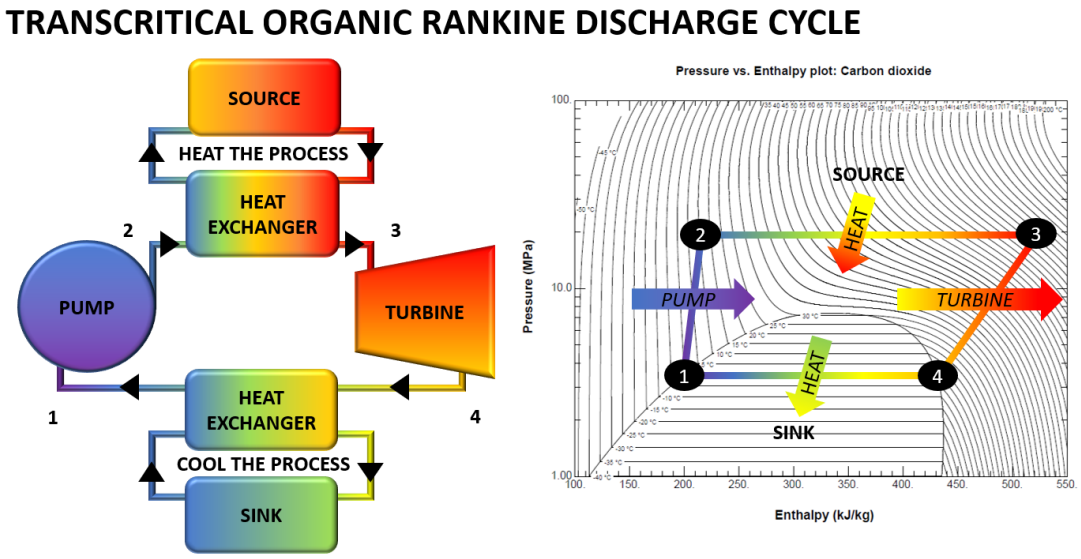

Figure-7 Transcritical Organic Rankine Discharge Cycle

4. THERMODYNAMIC ANALYSES: CO_2 EXPANDERS VS. JOULE-THOMSON VALVE

4.1. Carbon Capture, Utilization, and Storage (CCUS) Process

For a CCUS process, liquefaction is critical to efficient transport and storage of the captured carbon dioxide. A typical CO_2 liquefaction process involves the compression of the CO_2 gas stream to a supercritical state, cooling of the fluid to a subcooled liquid, and a pressure reduction to facilitate safe storage and transport of the saturated CO_2 mixture. This expansion is typically realized using a Joule-Thomson (J-T) valve. The J-T valve expands the liquid isenthalpically and does not remove any energy from the fluid, thus producing a saturated mixture containing a meaningful amount of vapor. This vapor can be recycled back through the system or used as a precooling medium depending on the configuration of the cycle, but it detracts from the efficiency of the process. Replacing the J-T valve with a liquid expander helps to mitigate this inefficiency by reducing the enthalpy of the liquid as it expands, creating a denser output condition. The enthalpy reduction is a result of angular momentum transfer to a shaft coupled to an electric generator, which converts the momentum into electrical energy that can be used to offset power demands of the plant. The added liquid throughput and extracted electrical power improve the efficiency of the liquefaction process significantly. An inline J-T valve downstream of the liquid expander is often used to isenthalpically expand the fluid to its final saturated state because the liquid expander is not meant to handle any vapor flow.

The expansion portion of a CO_2 liquefaction process is shown in Figure-8, highlighting the traditional expansion using only a J-T valve as well as an expansion process utilizing a liquid expander paired with an inline J-T valve. It can be seen that the liquid expander portion of the letdown process works to cool the fluid and reduce its enthalpy, while the J-T valves reduce the pressure isenthalpically. The enthalpy reduction realized by the expander directly correlates to an increase in fluid density and a decrease in fluid quality (vapor mass fraction), resulting in greater liquid throughput.

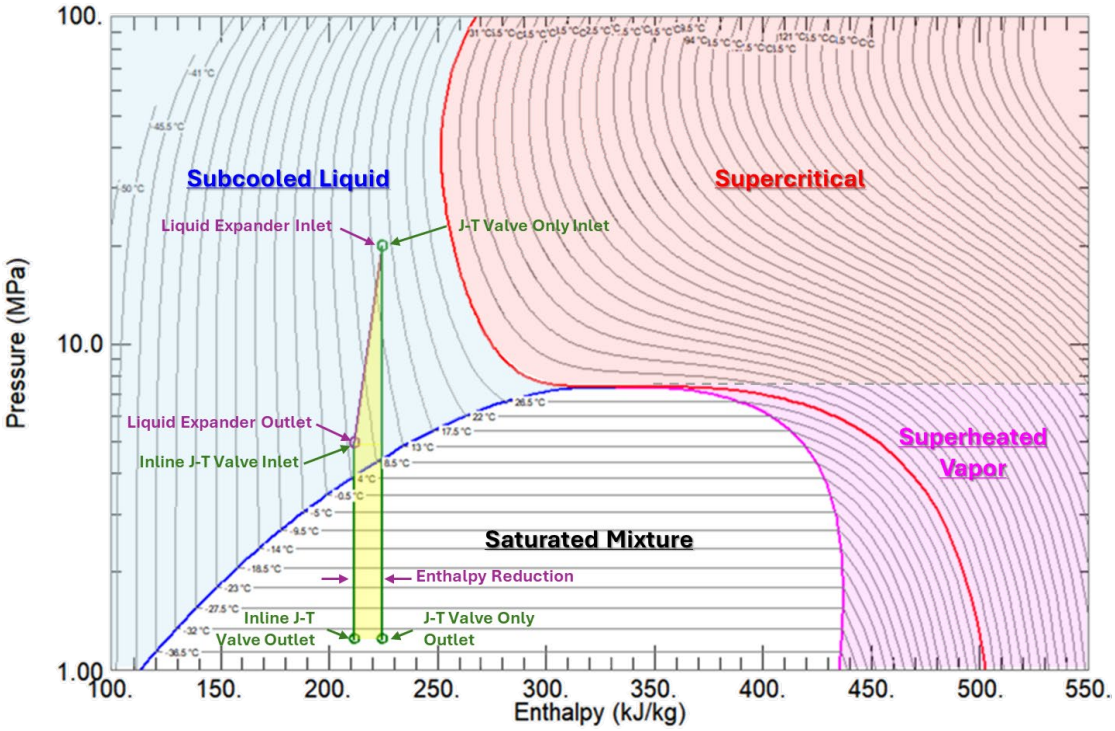

Figure-8 PH Diagram for CO_2 Liquefaction Letdown Process, Liquid Expander

A two-phase expander design is also being developed to remove the need for the downstream J-T valve and further improve the efficiency of the cycle by facilitating a greater drop in enthalpy as the fluid expands. The suitability of this new two-phase expander depends on process conditions and the ultimate goal of the cycle. In looking at the same process conditions mentioned previously - inlet pressure of 20 MPa, inlet temperature of 15°C, mass flow rate of 100 kg/s pure CO_2 - it is seen from Figure-9 that the two-phase expander is able to extract additional energy from the expansion into the two-phase region, further reducing the enthalpy and producing more liquid throughput.

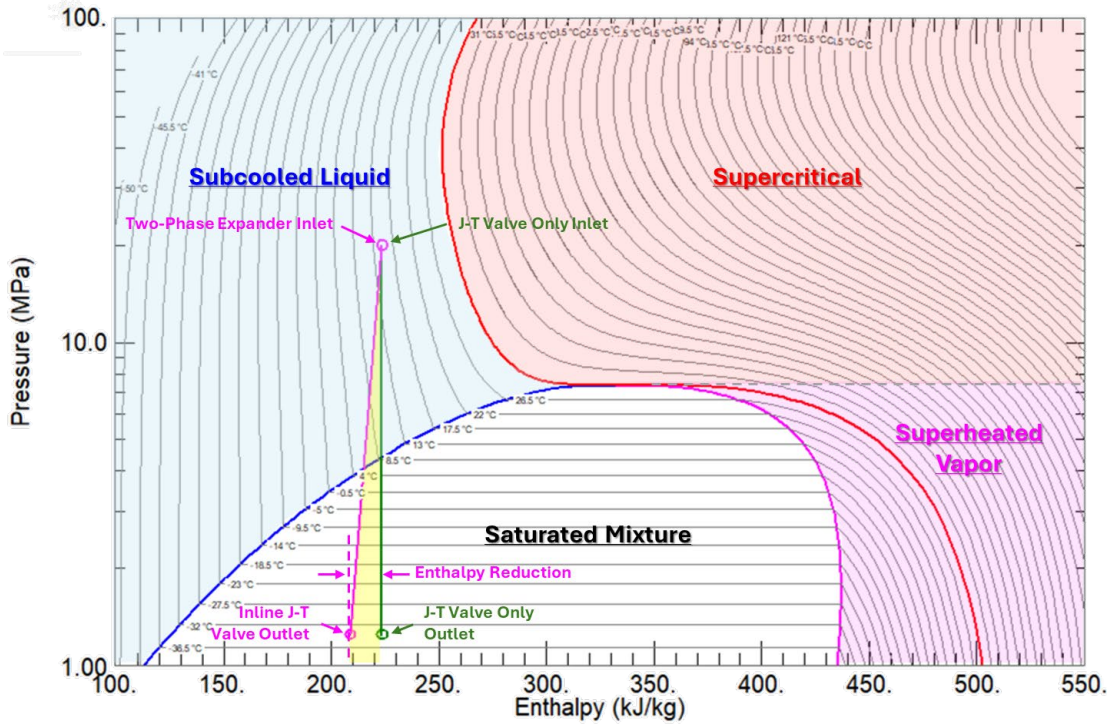

Figure-9 PH Diagram for CO_2 Liquefaction Letdown Process, 2-Phase Expander

4.2. Pumped Thermal Energy Storage (PTES) Process

During the charge cycle of a PTES process, the fluid is typically expanded using a Joule-Thomson (J-T) valve. The isenthalpic nature of the J-T expansion is inefficient, as no energy is extracted from the fluid. The round-trip efficiency of a PTES process is defined as the net work output during the discharge cycle divided by the net work input during the charge cycle, so any reduction in work input will improve the efficiency of the process. A liquid expander in lieu of the J-T valve can facilitate a reduction in work input by converting a portion of the fluid's energy to angular momentum. When coupled to a generator, this angular momentum can be extracted from the fluid in the form of electrical energy which can then be used to offset the work input from the compressor during the charge cycle. To quantify this reduction in input power, an example expansion process is defined for both a J-T valve and a liquid expander.

A PH-diagram is shown in Figure-10 for a CO_2-driven PTES charge cycle with a mass flow rate of 100 kg/s. The CO_2 begins at state 1 as a superheated vapor. It is then compressed, taking it into the supercritical region and increasing its temperature significantly. Once compression is complete, the CO_2 transfers its heat to the source via a heat exchanger, reducing its enthalpy and converting the CO_2 to a subcooled liquid. Once through the heat exchanger, the fluid pressure is reduced. The green line again shows the expansion across a J-T valve, and the purple line shows the same pressure letdown using a liquid expander. While the fluid enthalpy remains constant along the J-T valve expansion, it can be seen that the letdown using the liquid expander works to reduce the enthalpy of the fluid, converting its pressure energy to shaft power. This reduction in enthalpy directly correlates to useable electric power. Once expanded, the fluid gains heat from the sink, changing its phase from a subcooled liquid to a superheated vapor and returning it to state 1 to repeat the cycle.

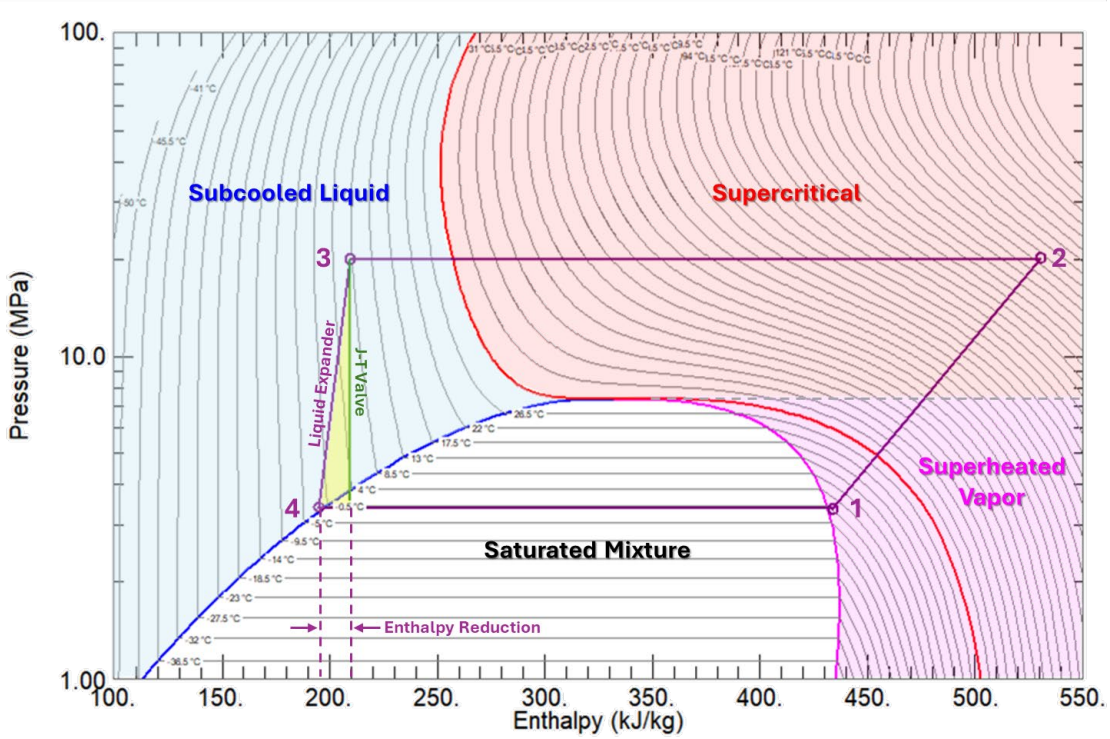

Figure-10 P-H Diagram for PTES Charge Cycle

5. EXPANDER DESIGN

5.1. Expander Design Overview

A typical sCO_2 expander assembly is shown in Figure-11. It consists of a submerged induction generator mounted on a common shaft with one or more Francis turbine runners. Unlike methane and mixed refrigerant expanders, which utilize aluminum alloy A356.0 for the runners, sCO_2 expander runners are cast stainless steel AISI 304 for increased strength. The density of sCO_2 is roughly twice that of methane, resulting in twice the differential pressure per stage and therefore twice the force per runner as compared with methane expanders. The runners are fed by stationary CNC-machined AISI 304 nozzle vanes. Deep-groove radial ball bearings carry only a radial load in this application, as thrust is entirely balanced by a Thrust Equalizing Mechanism (TEM®), which is similar to a balance drum but employs a variable orifice that constantly adjusts in response to operating conditions. TEM® function is verified with an axial probe during pre-shipment performance testing. Eddy probes mounted at the inlet side of the machine monitor the speed of the expander and are used for feedback in the case of VFD-driven expanders.

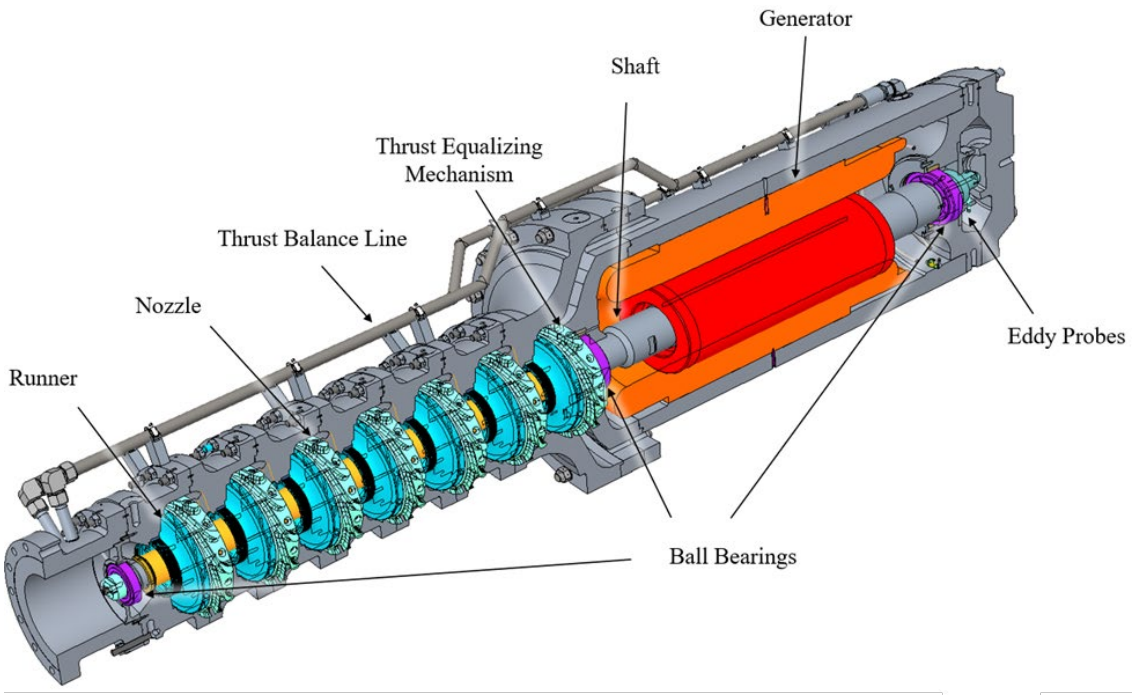

Figure-11 Typical sCO_2 Expander Assembly

5.2. Expander Operation

A typical sCO_2 flow schematic is shown in Figure-12. The main process flow path is indicated by green arrows. The process fluid enters the machine axially through the process inlet, limiting friction losses that would be incurred with a radial inlet. The velocity of the fluid is then increased by the nozzle vanes. Static pressure is converted into dynamic pressure, and this dynamic pressure is recovered by the runner. This exchange of static pressure for dynamic pressure is repeated across the entire stack of nozzles and runners. Enthalpy is removed from the sCO_2 in the form of shaft torque, which is converted to electrical energy in the submerged generator. A small amount of process fluid is diverted from the main flow path for generator cooling, thrust balance, and bearing lubrication, as indicated in Figure-12 by pale blue arrows. This diverted flow passes through the TEM®, balancing axial thrust, then proceeds through the main bearing, providing cooling and lubrication, through the generator air gap, providing cooling, and through the secondary bearing, providing lubrication. It then exits the machine through the process outlet by way of the thrust balance lines.

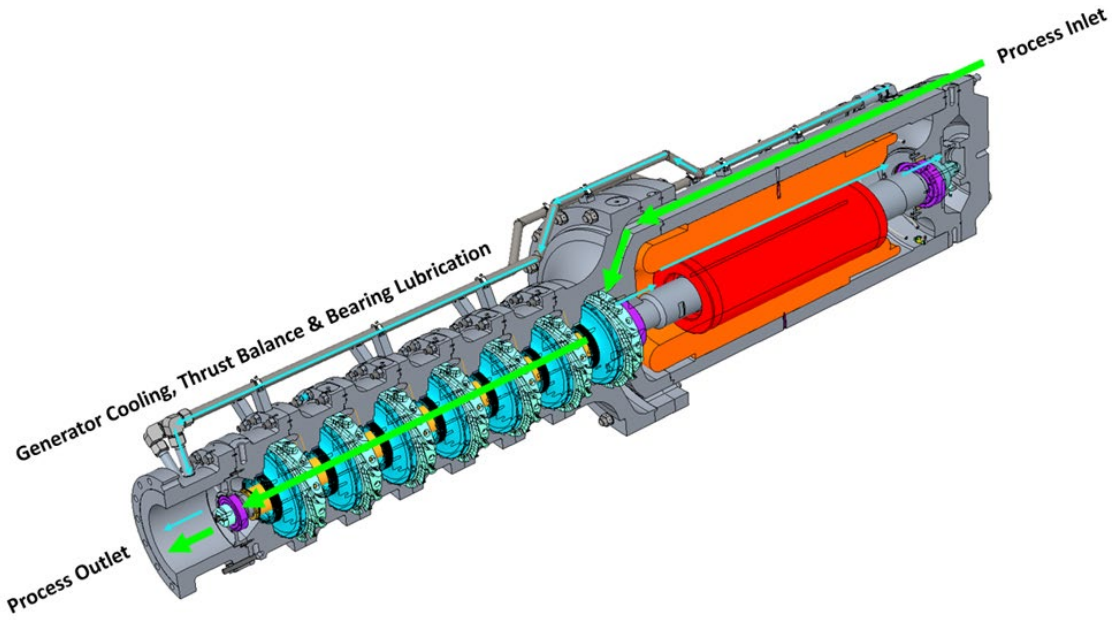

Figure-12 Typical sCO_2 Expander Flow Schematic

5.3. Expander Design Challenges

Supercritical CO_2 expanders are much like methane expanders in their design. The primary differences between the two include the temperature, density, and viscosity of the process fluid. Carbon dioxide liquid expanders tend to have a minimum operating temperature of around 0°C, while methane liquid expanders tend to have a minimum operating temperature of around -165°C. At -165°C, differential shrink rates between dissimilar materials can result in radial thermal stresses and changes in the alignment of axial components, and therefore require considerable attention during the design phase. At 0°C, concerns about differential shrink rates between materials of construction are minor. Elastomers perform well, and typical materials of construction for cryogenic pumps and expanders can be used, such as AISI 304 and Al 6061.

The density of CO_2 provides a unique challenge. Methane expanders are widely deployed and well known in liquefaction processes and mixed refrigerant loops. To a large extent, the same hydraulics may be used for CO_2 expanders, providing they have adequate strength. This requires the shift from aluminum alloy runners and nozzle vanes to AISI 304 runners and nozzle vanes, and an increase of the shaft diameter to account for the additional torque requirement associated with higher density. Additionally, the flow rates of CO_2 expanders tend to be lower than those of comparable methane expanders, leading to lower specific speeds and therefore lower attainable efficiencies. Higher pressures also require higher numbers of stages, resulting in rotordynamic considerations.

Bearing lubrication is achieved by means of the process fluid as shown in Figure-12. The minimum allowable viscosity for process-lubricated bearings is 0.045 cP, which is well below the viscosity of CO_2 within the operating range of expanders. Additionally, concerns about dry ice formation in the bearings can be dismissed by comparing the performance of actual operating methane expanders, which have typical minimum operating temperatures around -165°C, with CO_2 expanders, which have minimum operating temperatures around 0°C. The melting line of methane is shown in Figure-14. It can be seen that the pressure required to facilitate the formation of methane ice is 72.9 MPa at -165°C. CO_2, on the other hand, has a melting pressure

of 337.5 MPa at 0°C, which is 4.6 times as great as that of methane, as shown in Figure-13. This implies a factor of safety of 4.6 against dry ice formation if a CO_2 expander is built with the same Maximum Allowable Working Pressure (MAWP) as a methane expander.

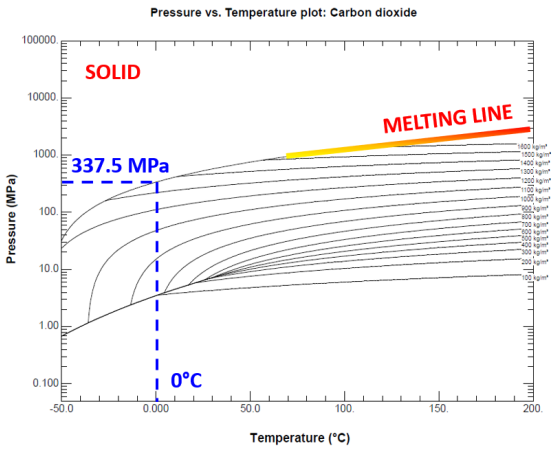

Figure-13 CO_2 melting line

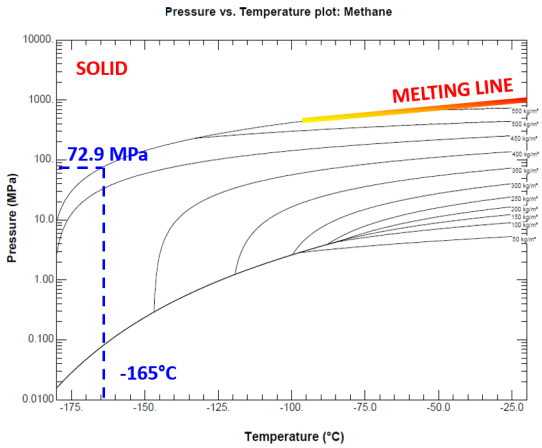

Figure-14 Methane melting line

5.4. Turbine Specific Speed

Specific speed is the most common dimensionless (unitless) parameter used in the determination of the turbine type and achievable efficiency. Formulation for specific speed can be obtained through utilization of Buckingham π theorem per the physical variables of the application. For pump applications, differential head (H), volumetric flowrate (Q), and rotational speed (n) are important variables to define pump characteristics and are used to obtain specific speed (N_s). Pump specific speed is determined by the following equation:

$$N_s = \frac{n\sqrt{Q}}{H^{3/4}}$$

It is important to pay attention to the units when calculating pump specific speed. Between metric and US unit systems, specific speed values vary significantly. This is because the form of the equation is not truly dimensionless, unless it is reduced by including gravitational acceleration. Pump specific speed is a useful guideline to determine the type of turbine. However, for some turbine applications, due to the importance of power generation, power (w) is taken into account in determination of specific speed and replaces the flowrate (Q) in the equation. Accordingly, turbine specific speed (n_s), can be calculated with the following equation:

$$n_s = \frac{n\sqrt{w}}{H^{5/4}}$$

Over the years, based on proven turbine applications and their operating conditions along with achieved efficiencies, turbine manufacturers established various specific speed maps to assist engineers in their selection and design of the hydraulic components. Since specific speed is a dimensionless parameter, specific speed maps can be applied to any turbine application, regardless of the physical size of the unit and the process. Besides the specific speed, other dimensionless numbers such as Reynolds Number, Mach Number, etc., shall be considered in the design and scaling of the turbomachinery. Maintaining these dimensionless parameters is key in scaling applications.

5.5. Turbine Specific Speed Map and Attainable Efficiency

Figure-15 covers the centrifugal type turbines and estimates efficiency based on a specific speed. This graph is produced based on the previously tested hydraulic expanders and the published data in the literature [4]. It should be noted the turbine specific speed map is prepared based on the specific gravity of 1. All of the shown efficiencies at each figure are hydraulic efficiencies that do not include any of the losses due to internal leakage, generator, etc. According to Figure-15, the turbines with a turbine specific speed (n_s) of 12 or greater are reaction turbines, which have a relatively higher flowrate, but also have lower head compared to impulse expanders. Reaction turbines utilize nozzle vanes to increase the velocity of the incoming flow to the turbine, while impulse turbines have jets to carry out the same function. Francis and Kaplan turbines are the most common reaction turbines used in turbomachinery applications. Francis turbines have a wide range of applications and are often used in liquid CO_2 applications. These expanders are capable of 90% hydraulic efficiency, with a resulting total efficiency of approximately 80%. Specific speeds range from 12 – 40 in US units.

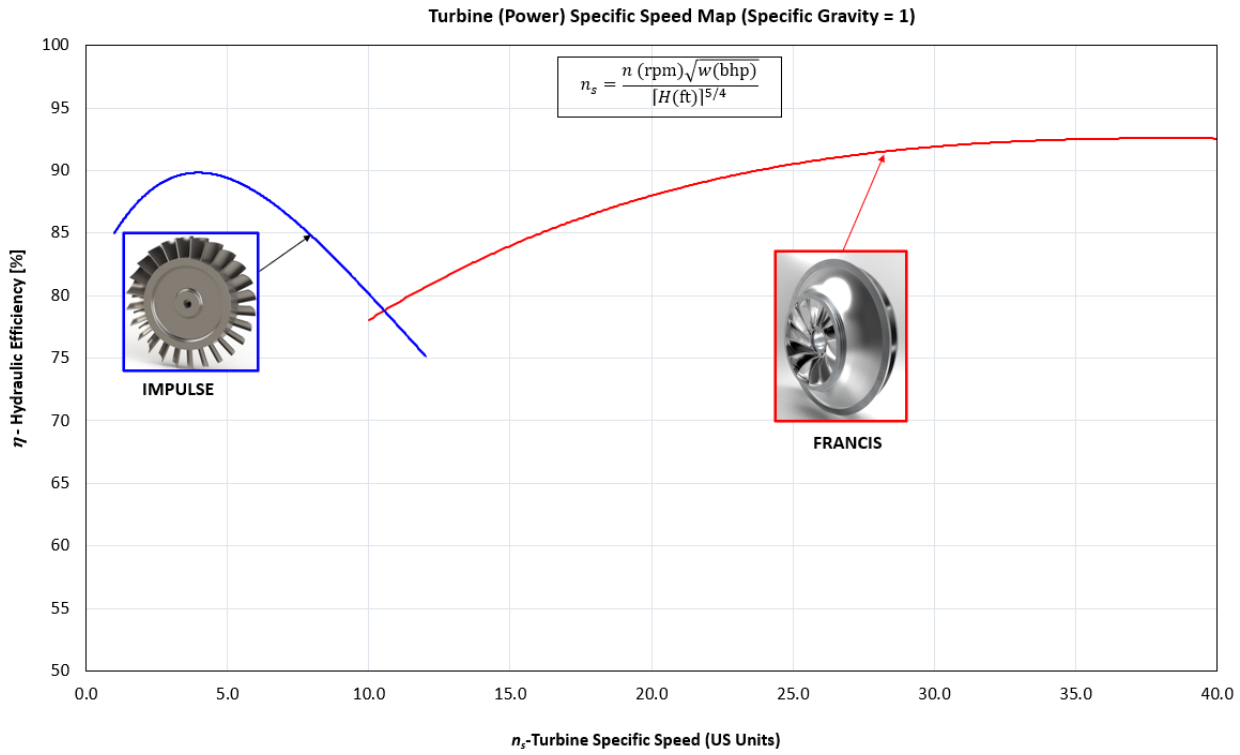

Figure-15 Hydraulic Turbine Expander Specific Speed Map.

Turbine specific speed is a guideline for design and process engineers to determine the turbine type and estimate the expected hydraulic efficiency of a turbine. The design of turbomachinery components, which is not limited to the design of hydraulic components, always plays an important role in achieving that efficiency. Design and process engineers often consider varying the rotational speed, increasing the number of stages, and even increasing the number of turbine units for a given total head and flow requirement of a process.

Rotational speed changes the specific speed linearly and is directly proportional to it. Speed also varies the head and flowrate of a turbine. The relationship between rotational speed and process parameters (head and flowrate) is defined by affinity laws for centrifugal turbine applications. It is often possible to vary the turbine speed by implementing variable frequency drives or by

changing the actual physical diameter of the turbine wheel. The impact on the rotordynamics, reliability of the turbine, and cost should be considered when examining a change to the rotational speed.

The most common way to adjust the specific speed is by increasing or decreasing the number of stages of the turbomachinery. This can be costly and there is always a limit to the number of stages that a turbine can handle. This limitation is set by the rotordynamic behavior of the turbomachinery and the maximum allowable pressure of the casings and related components.

Another method of adjusting the specific speed is to increase the number of turbines used in an application and the installation configuration of those turbines in that application. For relatively high head (pressure) applications, two or more turbines can be installed in series to increase the specific speed to a desired value while dropping the total pressure to the process needs. For applications with relatively high flow rates, turbines can be operated in parallel to reduce the specific speed of the turbine. It is often preferred to have a single turbine handle the process due to limitations of the footprint. Maintenance requirements and complexity of the system must also be taken into account if multiple turbines are to be operated in parallel or in series, due to the cost impact. Regardless, it may not be feasible to utilize a single turbine to meet the process needs.

5.6. Computational Fluid Dynamics (CFD) Simulations

Turbine expander performance in terms of pressure drop and efficiency is investigated for a range of flow rates to establish a turbine performance curve. To determine the turbine performance, ANSYS CFX software [5] is used to simulate the single stage of the turbine assembly that consists of a nozzle vane and a runner. The details of the simulations, governing equations, turbulence model and CFD grid geometry are reported in this section.

5.6.1. Governing Equations, Turbulence Model, and Boundary Conditions

For the purpose of CFD simulations, Reynolds-averaged Navier Stokes equations (RANS) are solved along with an appropriate turbulence model. Based on the simplicity and adequate accuracy to determine overall turbine performance, k-ε turbulence model is used in the present study. Table-1 outlines the boundary conditions and simulation details below. Thermodynamic properties of the liquid are defined as a function of temperature and pressure in accordance with published subcooling tables by NIST (National Institute of Standards and Technology) [6].

Table-1 Boundary Conditions and CFD simulation details

Inlet Boundary Condition:	Total Pressure in Stationary Frame: 2 MPa
Outlet Boundary Condition:	Mass Flow Rate: 90%, 100%, 105% and 110% of Rated Flow (Rated Mass Flow Rate: 100.98 kg/s, Vol. Flow Rate: 380 m^3/hr)
Fluid:	Carbon Dioxide at -5°C (23°F)
Rotational Speed:	3600 RPM (Applicable to Runner)
Interface Model between Rotating and Stationary Components:	Multi-frame of reference
Analysis Type:	RANS Steady State with "false" time scale
Turbulence Model:	k-ε turbulence model
Heat Transfer:	Isothermal at -5 °C
Density:	956.62 kg/m^3 (at Pressure: 3.1 MPa and Temperature: -5 °C)
Viscosity:	109.48e-6 Pa-s
Thermal Conductivity:	0.1152 W/m-K

5.6.2. CFD Model Geometry and Grid Structure

All hydraulic components—the runner and nozzle vane—were included in the CFD model to accurately predict the true turbine performance. The specific model geometry used for the CFD simulations is shown in Figure-16.

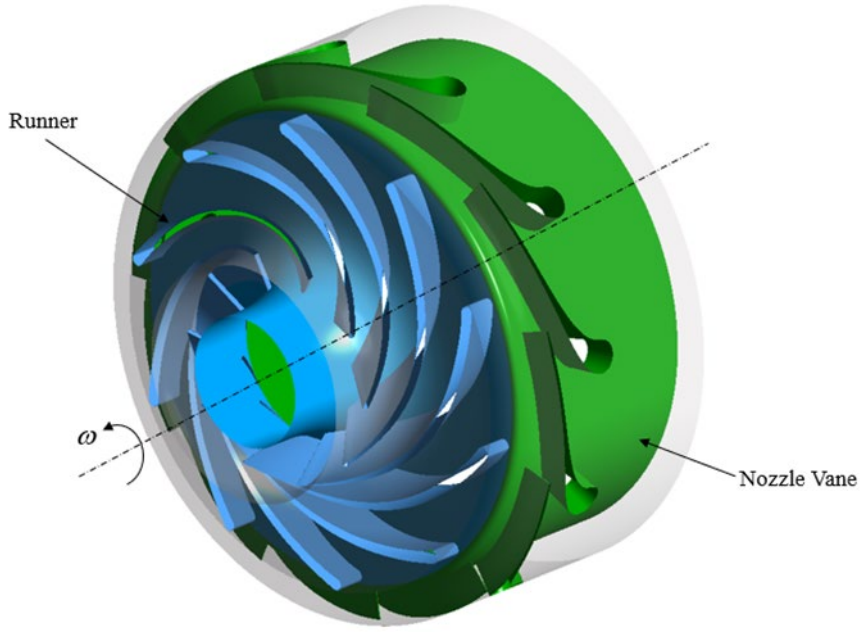

Figure-16 Turbine model – runner shroud is removed for clarity

Each hydraulic component is meshed using Turbogrid software to obtain a structured grid to ensure independence from mesh quality (or ensure mesh independence). In addition, a fine mesh resolution is implemented at wall sections to accurately capture the boundary layer effects. The grid structure quality is shown in Figure 17, using the nozzle vane as an example. A similar grid structure is used for both the runner and the nozzle vane.

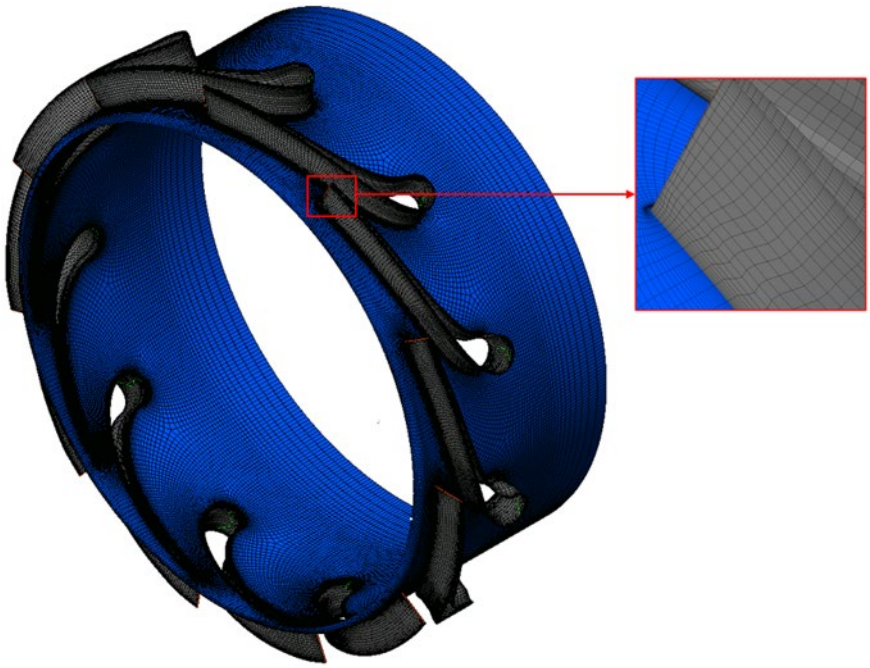

Figure-17 Sample grid structure and mesh quality of nozzle vane

To ensure convergence is reached by the iterative solver, the residuals for mass flow and momentum in each direction are monitored during each CFD run to confirm that the maximum Root Mean Square (RMS) residual is less than 1e-5. In addition, the turbine head is monitored during each run to ensure that the percentage variation of head is less than 0.5% over the last 250 iterations to further validate the accuracy of the simulations.

6. RESULTS AND DISCUSSION

6.1. CCUS – Production Gain and Power Recovery Comparison

Table-2 compares the liquid production and power generation for a liquefaction expansion process using the traditional J-T valve only, a liquid expander paired with a downstream J-T valve, and a two-phase expander. It's clear from the table that utilizing an expander, either liquid or two-phase, improves not only the process throughput of a liquefaction cycle, but also the efficiency of the process, as the electrical energy harvested from the process fluid can be used to offset power demands of the plant. Dropping the fluid pressure through a liquid expander paired with an inline J-T valve improves liquid throughput by 5.63% compared to a J-T valve-only expansion while also generating 1.14 MW of electrical energy from the liquid expander. When looking at expansion through the two-phase expander, this improvement in liquid throughput increases to 6.92% when compared to a J-T valve-only expansion, and the electrical power generation increases to 1.40 MW.

Table-2 CCUS Production Gain and Power Recovery Comparison

J-T Valve Only

Total Mass Flow Rate	100	kg/s
Vapor Mass Flow Rate	31.59	kg/s
Liquid Mass Flow Rate	68.41	kg/s
Fluid Quality (Vapor Mass Fraction)	0.32	-

Liquid Expander + Inline J-T Valve

Total Mass Flow Rate	100	kg/s
Vapor Mass Flow Rate	27.74	kg/s
Liquid Mass Flow Rate	72.26	kg/s
Fluid Quality (Vapor Mass Fraction)	0.28	-
Liquid Production Gain by Mass	3.85	kg/s
Liquid Production Gain by Percent	**5.63%**	**-**
Power Generation	**1.14**	**MW**

2-Phase Expander

Total Mass Flow Rate	100	kg/s
Vapor Mass Flow Rate	26.86	kg/s
Liquid Mass Flow Rate	73.14	kg/s
Fluid Quality (Vapor Mass Fraction)	0.27	-
Liquid Production Gain by Mass	4.73	kg/s
Liquid Production Gain by Percent	**6.92%**	**-**
Power Generation	**1.40**	**MW**

6.2. Pumped Thermal Energy Storage – Liquid Expander vs. J-T Valve

Typical process parameters for the expansion portion of the PTES charge cycle are shown in Table-3 for both the J-T valve and the liquid expander. While no power is extracted from the fluid using the J-T valve, the liquid expander recovers 1.22 MW during this letdown process. If this process uses a compressor with an isentropic efficiency of 85%, the utilization of a liquid expander in lieu of the typical J-T valve reduces the net power input required for the charge cycle by 12%.

Table-3 PTES Charge Cycle Expansion Process Comparison

Description	Units	J-T Valve	Liquid Expander
Mass Flow Rate	kg/s	100	100
Inlet Pressure	MPa (a)	20.0	20.0
Inlet Temperature	°C	8.0	8.0
Inlet Enthalpy	kJ/kg-K	209.4	209.4
Outlet Pressure	MPa (a)	3.4	3.4
Outlet Temperature	°C	-0.9	-1.4
Outlet Enthalpy	kJ/kg-K	209.4	196.6
Expander Efficiency	%	N/A	71.25
Power Generated	**MW**	**N/A**	**1.22**

6.3. CFD Simulation Results

Initially, differential pressure across single stage is reviewed for the turbine assembly. Since each stage is identical to each other in size and geometry, each stage essentially drops the same amount of pressure. To calculate the total pressure differential, stage pressure drop is multiplied with number of stages for each application. For this particular case, stage count is assigned as 7.

Figure-18 is showing the static pressure distribution across a single stage at the rated flow of the turbine at meridional plane. This plot is showing the area average of the pressure distribution that is distributed over to the meridional (primary flow) axis and plane. Differential pressure across the stage is calculated as 21.45 bar at rated flow. This corresponds to differential head of 227 m / stage.

Figure-19 shows the velocity plot in a blade-to-blade view. The nozzle vane effectively increases the fluid's momentum, and at the runner, this momentum is effectively reduced to gain torque. Ideally, the velocity at the runner outlet should be as close to zero as possible, with minimal to no swirl or rotation. Figure-20 shows the three-dimensional velocity plot to illustrate how well the angular momentum is increased across the nozzle vane and reduced across the runner, with minimal recirculation (swirl) at the runner discharge.

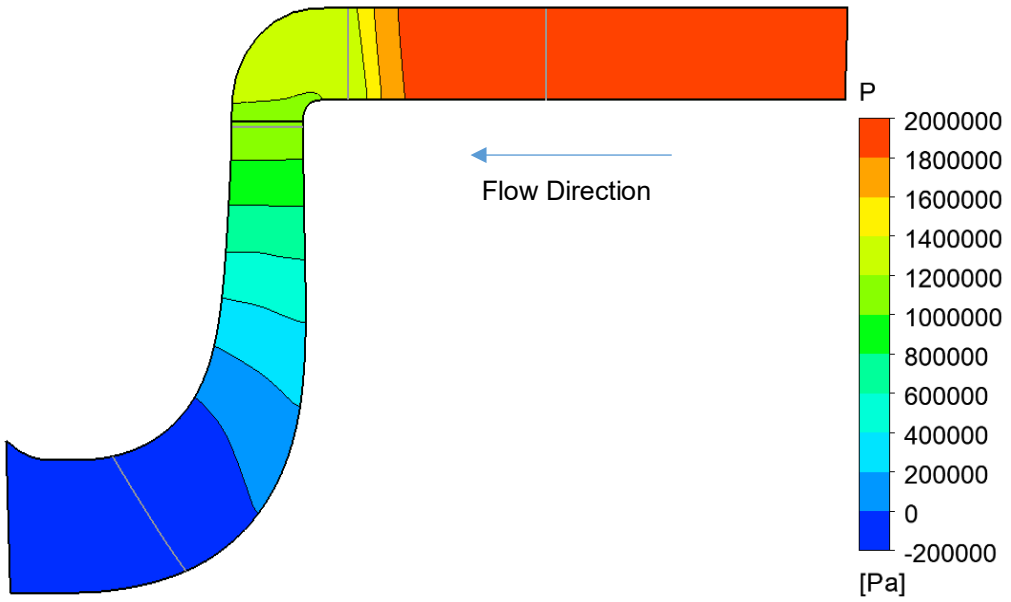

Figure-18 Static pressure distribution shown at meridional view at rated flow

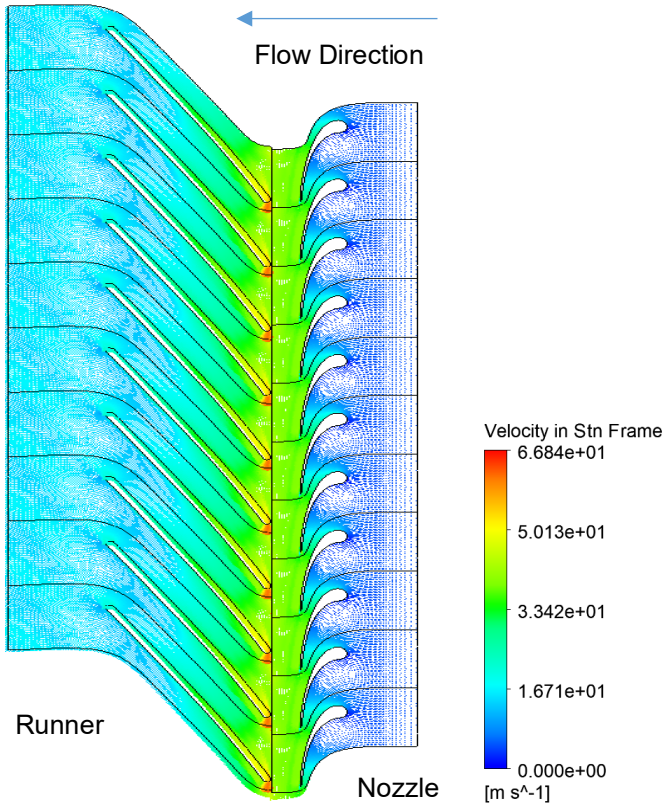

Figure-19 Velocity in stationary frame shown in blade-blade view at rated flow

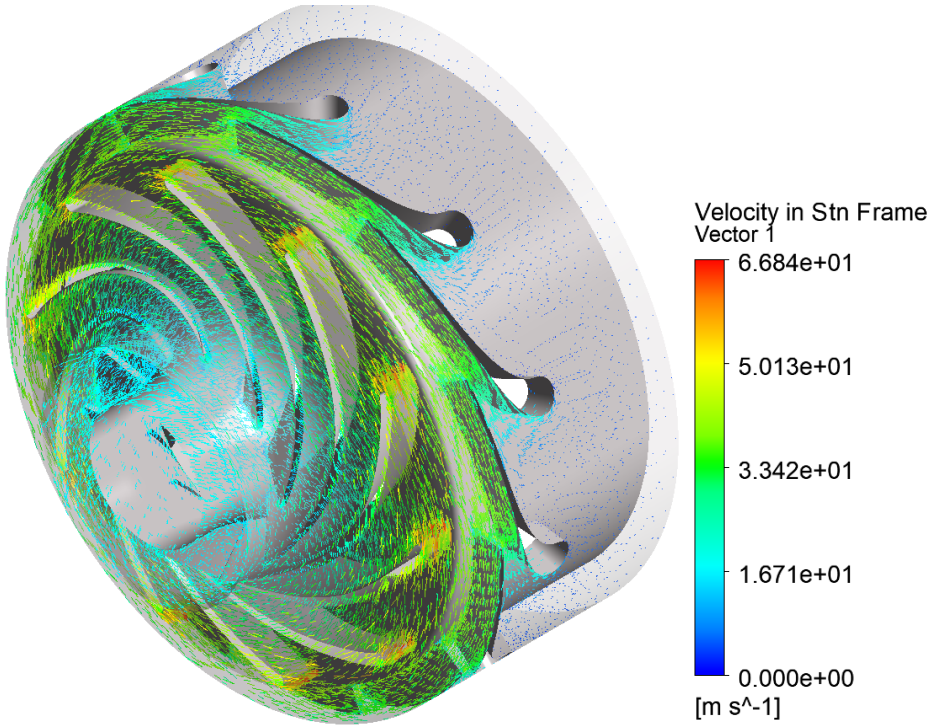

Figure-20 Fluid velocity vectors in stationary frame in three-dimensional view at rated flow

For hydraulic turbine applications, turbine performance is represented in terms of differential head and efficiency or power for a given volumetric flow rate. This is based on Annex C of the API 610 12th edition guidelines for hydraulic power recovery turbines (HPRT) [7]. Figure-21 is the performance curve for the turbine expander with actual test data and CFD simulations, prepared based on the guidelines by API 610 for a turbine performance curve. It should be noted that the process fluid is assumed to be incompressible, with a negligible density variation that is typically less than 5% between the turbine expander inlet and outlet conditions. The turbine performance curve includes head and efficiency for rated, maximum, and minimum speeds. Performance at various speeds is calculated based on the established affinity and scaling laws [8]. CFD simulation results are shown in diamond-shape markers and overlaid on the actual normalized test data. According to Figure-21, the CFD performance predictions are slightly higher than the actual test results. This is attributed to the leakage and losses associated with the thrust balancing system, generator cooling, and stage back leakages.

It should be noted that turbine expander performance curves are prepared by taking the total efficiency into account. The total efficiency includes the efficiency of the hydraulic components and the electrical generator. A generator efficiency of 90% is assumed in CFD simulations for the calculation of total efficiency. Hydraulic efficiency is calculated based on the mechanical power input to the expander (determined by flow rate and differential pressure) and the resulting output power (based on shaft torque).

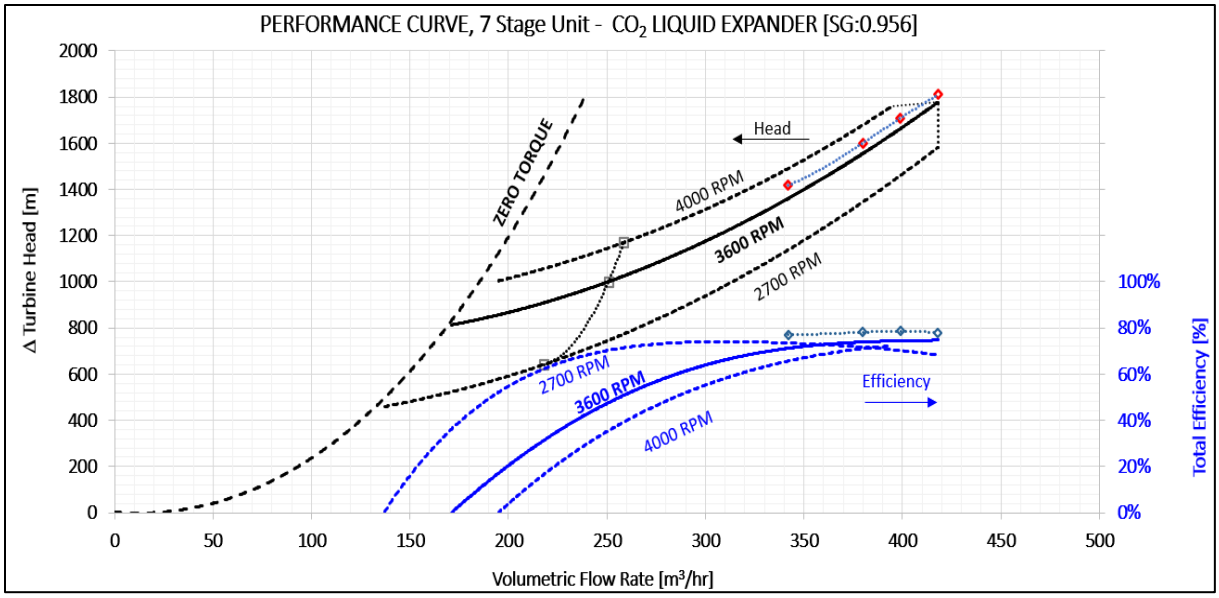

Figure-21 Turbine Performance Curve with CFD results shown in diamond markers

7. CONCLUSION

As global power demand continues to grow, global power supply must do the same. In order to maintain long-term global climate stability, the increase in global power supply must not be accompanied by an increase in greenhouse gas emissions. Carbon capture, accomplished through the amine scrubbing, membrane separation, and cryogenic capture processes, will continue to facilitate the reduction of anthropogenic CO_2 emissions. CO_2 expanders will play an increasingly vital role in the reduction of liquefaction process power consumption and improve liquid throughput. These expanders are built upon field-proven LNG turbine technology and will not only replace Joule-Thomson valves in liquefaction processes, but also will act as key components in transcritical and supercritical PTES applications. Time-tested parameters such as turbine specific speed map the achievable efficiencies of these machines, while modern computational methods such as CFD allow the rapid analysis and improvement of this technology for the next generation.

8. REFERENCES

[1] United States Environmental Protection Agency, "Inventory of U.S. Greenhouse Gas Emissions and Sinks," 1 July 2025. [Online]. Available: https://www.epa.gov/ghgemissions/overview-greenhouse-gases#overview.

[2] K. Brun, T. Allison, R. Kurz and K. Wyagnt, Energy Transport Infrastructure for a Decarbonized Economy, Cambridge: Elsevier, 2025.

[3] J. McTigue and P. Farres-Antunez, "Pumped Thermal Electricy Storage with Supercritical CO2 Cycles and Solar Heat Input," in *2019 Solar Power and Chemical Energy Systems Conference (SolarPACES)*, Daegu, South Korea, 2019.

[4] K. Nichols, "How to Select Turbomachinery for Your Application," [Online]. Available: http://www.barber-nichols.com/sites/default/files/wysiwyg/images/how_to_select_turbomachinery_for_your_application.pdf. [Accessed 2025].

[5] Ansys, *Ansys Workbench R2 (v242),* 2024.

[6] National Institue of Standards and Technology, "Thermophysical Properties of Fluid Systems," 2025. [Online]. Available: https://webbook.nist.gov/chemistry/fluid/.

[7] American Petroleum Institute, *Centrifugal Pumps for Petroleum, Petrochemical and Natural Gas Industries (API Standard 610, 12th ed.),* 2020.

[8] J. Gulich, Centrifugal Pumps, New York: Springer, 2010.

[9] E. Lemmon, I. Bell, M. Huber and M. McLinden, *NIST Reference Fluid Thermodynamic and Trasport Properties Database (REFPROP) Version 10,* 2013.